Biofilm 7 (2024) 100186

Contents lists available at ScienceDirect

Biofilm

journal homepage: www.sciencedirect.com/journal/biofilm

UV emitting glass: A promising strategy for biofilm inhibition on transparent surfaces

Leila Alidokht [a], Katrina Fitzpatrick [a], Caitlyn Butler [a], Kelli Z. Hunsucker [b], Cierra Braga [b], William A. Maza [c], Kenan P. Fears [d], Marieh Arekhi [a], Mariana Lanzarini-Lopes [a,*]

[a] Environmental and Water Resource Engineering, Department of Civil and Environmental Engineering, University of Massachusetts Amherst, MA, USA
[b] Center for Corrosion and Biofouling Control, Florida Institute of Technology, Melbourne, FL, USA
[c] Chemistry Division, U.S. Naval Research Laboratory, Washington, DC, USA
[d] Center for Biomolecular Science and Engineering, U.S. Naval Research Laboratory, Washington, DC, USA

ARTICLE INFO

Keywords:
Biofilm prevention
UVC disinfection
Scattering nanoparticles
Transparent surfaces
Surface hygiene
Antimicrobial coatings
Marine environment

ABSTRACT

Marine biofouling causes serious environmental problems and has adverse impacts on the maritime industry. Biofouling on windows and optical equipment reduces surface transparency, limiting their application for on-site monitoring or continuous measurement. This work illustrates that UV emitting glasses (UEGs) can prevent the establishment and growth of biofilm on the illuminated surfaces. Specifically, this paper describes how UEGs are enabled by innovatively modifying the surfaces of the glass with light scattering particles. Modification of glass surface with silica nanoparticles at a concentration 26.5 μg/cm^2 resulted in over ten-fold increase in UV irradiance, while maintaining satisfactory visible and IR transparency metrics of over 99 %. The UEG reduced visible biological growth by 98 % and resulted in a decrease of 1.79 log in detected colony forming units when compared to the control during a 20 day submersion at Port Canaveral, Florida, United States. These findings serve as strong evidence that UV emitting glass should be explored as a promising approach for biofilm inhibition on transparent surfaces.

1. Introduction

Biofouling on the exterior surface of marine vessels and equipment creates significant operational, functional, and financial hurdles. Biofilm is a consortium of microorganisms immobilized in a matrix of extracellular polymeric substances (EPS). Biofilm growth and the biocorrosion associated with surface-attached biofilms can damage oceanographic equipment and decrease the optical transparency of windows used for cameras and communications devices. Biofilm formation costs the United States Navy Fleet between 180 and 260 million dollars per year [1]. Increased surface roughness increases hydraulic drag and fuel consumption, while corrosion causes significant irreparable damage to the vessel's components [2]. Moreover, ship biofouling is an important mechanism for the translocation and introduction of non-native species throughout the world [3], which can impact various economic, ecological, societal, and cultural values.

Current approaches for biofilm prevention on ship hulls involve the application of antifouling biocidal or non-biocidal coatings. Biocidal coatings employ an active agent to kill fouling organisms. Due to their high persistence and toxicity, antifouling biocides adversely affect the nontargeted fouling organisms and can therefore compromise ecosystems [4]. Non-biocidal coatings include fouling-resistant and fouling-release coatings [4,5]. To fulfill their purpose, these coatings must exhibit long-term mechanical and chemical stability, ease of application and proper adherence to the surface of interest while preventing and detaching a wide variety of fouling organisms. Designing a successful coating is a time- and cost-intensive process and requires interdisciplinary work to connect physical-chemical concepts to biological phenomena [6].

Germicidal ultraviolet radiation between 250 and 280 nm (UVC radiation) is chemical-free and can prevent marine biofilm formation at extremely low irradiance [7]. UVC radiation prevents organism replication, growth, and infection by damaging the cell's DNA, RNA, and protein structures [8]. Recently, surface exposure to external UVC

* Corresponding author.
E-mail addresses: lalidokhtakh@umass.edu (L. Alidokht), kfitzpatrick@umass.edu (K. Fitzpatrick), csbutler@umass.edu (C. Butler), khunsucker@fit.edu (K.Z. Hunsucker), cbraga2012@my.fit.edu (C. Braga), william.maza@nrl.navy.mil (W.A. Maza), kenan.fears@nrl.navy.mil (K.P. Fears), marekhi@umass.edu (M. Arekhi), marianalopes@umass.edu (M. Lanzarini-Lopes).

https://doi.org/10.1016/j.biofilm.2024.100186
Received 25 October 2023; Received in revised form 20 February 2024; Accepted 20 February 2024
Available online 28 February 2024

radiation has been applied in the marine field to prevent biofouling formation on multiple surfaces (Table 1). However, the inability to distribute adequate light across the surface of interest is the main limitation of using UV light for biofilm prevention in marine environments and large surface areas. Light intensity decays as it moves away from the point source due to diverging of rays and attenuation from scattering and absorption [9]. For example, as turbidity of water increases the amount of UV light that can reach a surface from the same source decreases [10].

Here we present an approach to glow UV light from the inside of windows to prevent biological attachment and growth on the surface. Glass substrates such as windows can be modified to externally emit UV light and prevent biological growth on their surface. The core technology is based on the use of nanoparticle-enabled waveguides 9,20. UVC light (265 nm), launched from a LED, travels through the glass core and is scattered by the nanoparticles on the surface, resulting in side-emission into its surrounding water or air. When total internal reflection (TIR) occurs within a waveguide, an evanescent wave is generated through the sides of the substrate [21,22]. By adding scattering nanoparticles onto the glass surface, we disturb the electromagnetic wave, causing the light to leave (leak out) the waveguide substrate, resulting in side-emission and outcoupling of UVC radiation into the surrounding medium.

We have previously demonstrated the ability to obtain "glowing" UV light from a cylindrical waveguide for biofilm prevention. We fabricated side-emitting optical fibers (SEOFs) by modifying a traditional optical fiber with highly scattering silica (SiO_2) particles (>200 nm in diameter) and attaching a UV LED (265 nm) to the fiber [9,23]. SEOFs can effectively inactivate planktonic bacteria (2.9 log inactivation of *Escherichia coli* at a delivery dose of 15 mJ/cm^2) [9] and prevent bacteria growth on surfaces (inhibition zone of 3 cm at a delivery dose of ~4.3 mJ/cm^2) [23].

In this study, we aimed to provide proof of concept that UV surface-emitting (glowing) glass can prevent marine biofilm formation on a transparent surface. A UV emitting glass (UEG) (Provisional Patent US Serial No. 63/506,985) was fabricated to emit UV light throughout its length (Fig. 1). The UEG was deployed in a marine environment for 20 days to assess the ability of UEGs to prevent biofilm when compared to a similar non-UEG control.

2. Methods

2.1. Fabrication of UV-emitting glass (UEG)

UV transparent quartz slides measuring 24 × 110 mm and 2 mm thick were modified to emit UV light through a three-step method. Step 1 involved cleaning the slides at room temperature by immersing them in acetone (99.5%) and sonicating the solution for 10 min to remove any deposits from the exposed surfaces. Step 2 includes the application of scattering nanoparticles onto the cleaned slides by electrostatic deposition. Aminated silica spheres suspended in ethanol with a diameter of 200 nm (nanoComposix, San Diego, CA, 10 mg/mL, SIAN200), were selected due to the low absorptivity and high scattering coefficient at 265 nm. Positively charged aminated spheres facilitated the attachment to the negatively charged glass slide surface. The nanoparticle suspension was sonicated for 10 min before application. Approximately 700 μL of the suspension was gently pipetted onto the slide to uniformly cover the 26.5 cm^2 surface area of the slide before drying for 2 h. UEGs with different mass coverage (μg/cm^2) of nanoparticles on the slides were fabricated by diluting the nanoparticle suspension with Ethyl Alcohol 100% (Decon Laboratories, Inc. PA). In Step 3, the slide was coated with Cyclic Transparent Optical Polymer (CYTOP™) (AGC Chemicals, USA) by semi-print screen technique. Following sonication for 10 min, 300 ± 20 μL polymer was dragged along the exposed facet of the glass slide using the round edge of a razor blade and dried at room temperature overnight. The polymer serves to (1) act as a cladding to the glass, (2) protect the glass core, and (3) fixate the nanoparticles close to the substrate. Therefore, a minimum coating thickness was desired, while ensuring complete coverage of the substrate and nanoparticles. CYTOP is a fluoropolymer characterized by its amorphous structure, allowing for remarkable transparency (>95% for 1 mm) over a wide spectral range (200–2000 nm), and is well-suited for functioning as an optical thin film coating.

The thickness of the coating material was measured by AFM profilometry using a Jupiter XR Atomic Force Microscopy (AFM) (Oxford Asylum Research, UK) across a scratch made by a brass pin on the coating layer. When scanning, measurements of the material derived from scratching was avoided by selecting areas free of debris when possible. The instrument was operating in tapping mode using SuperSharp PointProbe-Plus®-NCHR Silicon tips (NANOSENSORS™, Switzerland). These measurements were repeated four times at different locations, and the average value is reported.

2.2. Establishing optical transparency vs. UV emission profile

A series of 12 slides were prepared to investigate the optical transparency and UV emission profile resulting from changes in nanoparticle concentration. The first six slides were fabricated with varying concentrations of nanoparticles, including 265, 132.5, 53, 26.5, 2.65, and 0 μg/cm^2, prepared from 1:0, 1:2, 1:5, 1:10, 1:100, and 0:1 dilutions of nanoparticle suspension, respectively. Each of these slides was then coated with a polymer layer. The remaining six slides were coated with nanoparticles at the same mass coverage, without the polymer coating. The fabricated UEGs were subsequently characterized for their optical transparency and UV emission profiles.

The optical transparency of the slides was measured by the U.S. Naval Research Laboratory (NRL) by positioning a collimated light source in front of the substrate followed by a detector behind it. Measurements were carried out over a spectral range of 400–2500 nm using Flame (Flame-T-XR1-ES, Ocean Insight, USA) and NIR Quest (NQ512–2.5, Ocean Insight, USA) spectrometers working in tandem. The light sources used in the measurements (DH-2000-FHS-DUV-TTL for

Table 1
Summary of the most recent applications of UVC for prevention of biofilm formation on surfaces.

Source of UVC	Target bacteria	Surface material	Ref.
LED	Biofilm-bound *Pseudomonas aeruginosa*	Clear polycarbonate coupons	Gora et al. [11]
LED	*Escherichia coli*	Fused silica glass	Torkzadeh et al. [12]
Lamp	Marine bacteria	Polycarbonate Stainless steel	Richard et al. [13]
LED	*Pseudomonas* spp., *Legionella* spp., Mycobacteria	Polycarbonate coupons Quartz coupons	Ma et al. [14]
LED	Marine bacteria	Aluminum plates	Abhishek et al. [15]
Lamp	Marine bacteria	Borosilicate microscope slides	Braga et al. [16]
Lamp	Marine bacteria	Steel plate coated with an ablative copper antifouling and a silicone fouling release coating	Braga et al. [17]
Lamp	Marine bacteria	Aluminum sheet coated with polydimethylsiloxane	Cagnola et al. [18]
LED	Marine bacteria	Perspex test plate	Ryan et al. [19]

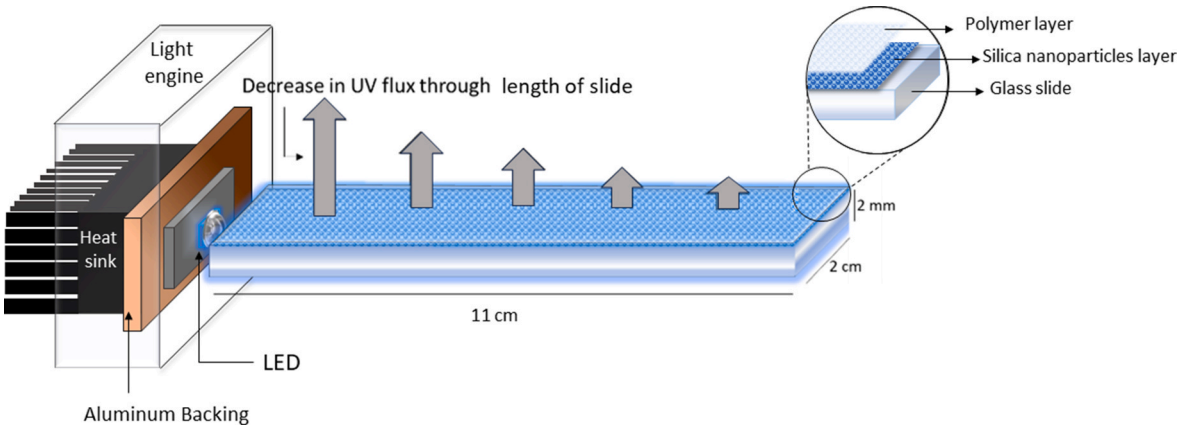

Fig. 1. Schematic illustration of UV emitting glass (UEG) and light engine.

Vis, and HL-2000-HP-FHSA for NIR, respectively; Ocean Insight, USA), were directed onto the slide using a sample 74-ACH adjustable collimating lens holder (Ocean Insight, USA), modified with custom-made 3D printed panel brace and 74-UV collimating lenses (Ocean Insight, USA). The intensity of light passing through the slides was collected and recorded using the OceanView software package, and the percent of transmission was calculated during data processing using the MATLAB software package using control (uncoated) slides for background signals. Visual Resolving Power evaluations were conducted using a USAF 1951 Optical Calibration Target printed at 8.5" × 11" scale. Comparisons were made to an uncoated blank slide.

The UVC emission profile measurements were conducted using a spectroradiometer (AvaSpec-2048L, Avantes, Louisville, CO USA), calibrated over the wavelength range of 200–1100 nm. UEGs were placed in a slide holder case (section 2.3.1) in a perpendicular position to the UV LED lamp. The UV irradiance (μW/cm^2) was measured along the length and perpendicular distance from the UEG surface by placing the spectroradiometer's sensor tip (5 mm^2) normal to the surface at a 1 mm distance. Intensity was measured at distances of 1, 3, 5, 7 and 9 cm from the UV LED. The total irradiance was obtained by integrating the output spectrum over 240–300 nm. Triplicate measurements were taken at each position along independent UEGs. The output intensity was corrected for the dark data for correct full-width half maximum (FWHM) calculations. The reflectance of light by the benchtop was measured by inverting the spectroradiometer tip away from the light source and normal to the benchtop surface. No signal was measured indicating that the surrounding material had no influence on the light distribution profile.

2.3. Submersion

2.3.1. Case design

The submersion cases were 3D-printed by UMass Advanced Digital Design and Fabrication (ADDFab) 3D printing facilities (STL files and instructions for assembly are available from the authors at reasonable request). The cases were printed on nylon-12 (PA2200) with a density (laser sintered) of 930 kg/m^3 and certified for biological tests (USP class: VI). Each case contained six chambers housing two control slides and 4 UEG (nanoparticles concentration: 26.5 μg/cm^2) (Fig. 2). The controls included polymer-only slides with no UV. Each chamber dimension was approximately 25 mm × 3 mm x 100 mm. 3D printed side brackets secured one side of the slide against the chamber so that only one side of the slides was exposed to the marine environment and therefore to biofouling.

2.3.2. Coupling UV LED to UEG

The water-sealed top compartment of the 3D-printed cases were designed to accommodate the LED strip, aluminum backing, heat sink, and electrical connections and wiring (Fig. 2). Strips of four UV LEDs with 30-degree lenses and emission peak of 265 nm were acquired from Violumas, San Diego, CA. The LED strip was screwed to the aluminum backing and placed in the light housing space. A butt-coupling approach

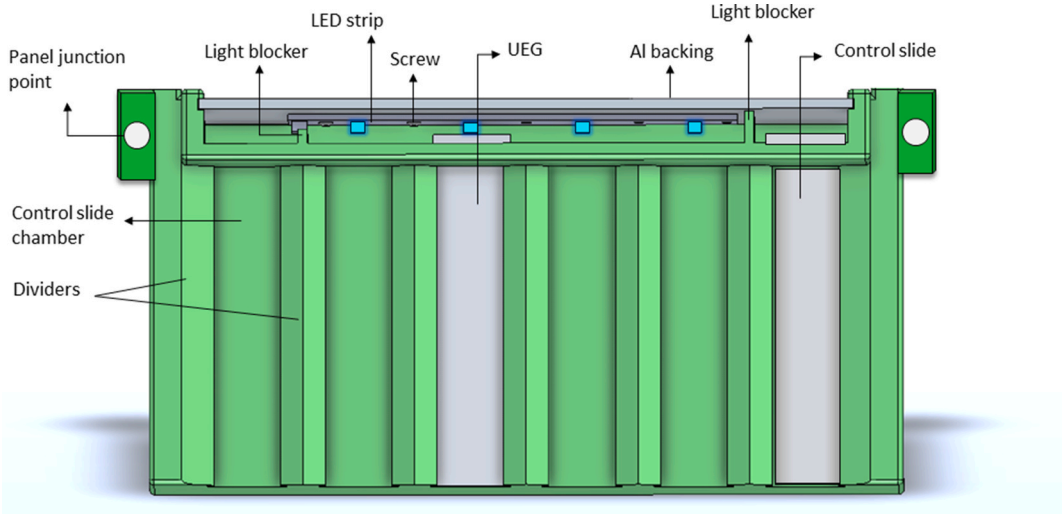

Fig. 2. Schematic of the submersion case.

was used between LED and UEGs. The UEGs were secured inside the light engine by a silicone binder.

The LEDs produce up to 2–4 J/s of heat. During submersion, the marine environment was used as the heat sink. However, during UV profile measurements, four 22 mm × 22 mm x 7 mm anodized aluminum heatsinks (Easycargo, Amazon, Seattle, WA USA) were attached to the aluminum backing to assure proper semiconductor cooling. A fan (HT 900, Honeywell, Charlotte, NC USA) was directed to the LED to further dissipate heat. A 700 mA current was delivered to the UV LEDs for all experiments. The output wattage of each LED was 71 mW. During submersion, the light engine was sealed with a silicone binder to avoid water infiltration. The cases were connected to an external power source, and all electronics except the LEDs were kept above water. Cases were mounted to a submersion platform via panel junction points and submerged on January 20th, 2023, at Port Canaveral, Florida, United States. A total of twelve slides were submerged in two submersion cases for 20 days.

2.4. Biofilm formation analysis

2.4.1. Visual assessment of biofilm formation

American Society for Testing and Materials (ASTM D6990) standard was used to qualitatively assess biofouling coverage when UEGs and control slides were subjected to immersion conditions in a marine environment [24]. The assessment was performed in the field immediately after slide retrieval to estimate the total coverage of biofilm. Each slide was photographed and divided into a grid arrangement to define observation areas. Prior to retrieval, submersed cases were gently agitated to remove any silt or loosely attached material from the slide's surface.

2.4.2. Pour plate method (culturable cell quantification)

After retrieval, each slide was divided into 3 equal parts, namely p_1, p_2, and p_3. Among these parts, p_1 was closest to the UV LED, p_2 middle, and p_3 the part furthest from the LED. Biofilms were aseptically extracted from the slide surface using a sterile cell scraper and executing a reproducible side to side brushing pattern. The extracted biofilm was suspended in a 10 mL sterile phosphate buffer solution (PBS) to prevent osmotic shock and dispersed via combined action of vortex-ultrasound-vortex (each for 1 min). PBS was prepared by dissolving one BupHTM PBS Pack (Fisher Scientific, USA) in a final volume of 500 mL deionized water. The resulting suspension was designated as BS (biofilm suspension).

To prepare Marine Agar, 37.4 g of Marine Broth powder (Sigma-Aldrich, 76,448) and 10 g of Agar (Sigma-Aldrich, A1296) were dissolved in 1 L of deionized water while being heated and continuously mixed. The solution was boiled for 1 min and autoclaved at 121 °C for 1 h. Biofilm suspension obtained from control slides were subjected to a four-fold dilution by combining 1 mL BS with 3 mL sterile phosphate buffer solution. For the BS obtained from UEGs, no dilution was performed. A total of 1 mL of each diluted/un-diluted suspension was added to a sterile Petri dish, followed by the addition of 20 mL of liquified marine medium acclimatized at 48 ± 2 °C. The plates were thoroughly swirled to ensure proper mixing of the liquid medium with the sample and were left undisturbed in a biosafety hood until the medium was completely solidified. Incubation of the plates was carried out at 37 ± 1 °C for 24 h, and the colony forming units (CFU) per cm^2 was recorded as the resulting data. All opaque growth spots were counted as a colony. Statistical consistency between dilutions indicated lack of contamination.

2.4.3. Live/dead analysis

To evaluate the viability of bacterial populations based on cell membrane integrity, the LIVE/DEAD BacLight™ Bacterial Viability Kit (Invitrogen, USA) was utilized. This kit enables the differentiation of cells with compromised membranes, with dead or dying cells stained red and cells with intact membranes staining green. Sample preparation and staining procedures followed the manufacturer's instructions provided with the BacLight™ Assay Kit.

Initially, 6 mL of the biofilm suspension was transferred into a sterile centrifuge tube and centrifuged at 10,000×*g* for 10 min. The supernatant fluid was carefully removed, and the resulting pellet was resuspended in 20 mL buffer solution. After vortexing for 1 min, the suspension was incubated at room temperature for 1 h. Subsequently, the suspension was centrifuged at 10,000×*g* for 10 min and the pellet was resuspended in another 20 mL buffer solution. Once again, the sample was vortexed and centrifuged as described above. No dilution occurred during washing.

The harvested cells were suspended in a 2 mL buffer solution and vortexed for 1 min. From this suspension, 1 mL of the sample was mixed with 3 μL of the LIVE/DEAD BacLight Kit mixture containing a 1:1 ratio of SYTO™ 9 nucleic acid (final concentration: 29.91 μM) and propidium iodide (PI) (final concentration: 4.99 μM) and incubated in the dark for 15 min at room temperature. To visualize the stained bacterial cells and determine their viability, 5 μL of the stained bacterial suspension was pipetted onto a microscope slide and covered with a coverslip. Images were captured by fluorescence microscope (AMG EVOS FL, USA), from eight randomly selected areas of each microscope slide. Green fluorescent protein (GFP) images were used to count live images and red fluorescent protein (RFP) images were used to count dead cells. The number of live and dead cells was recorded, and the mean values were reported.

2.4.4. Protein and DNA analysis

For the quantification of unbound proteins, 3 mL of the biofilm suspension was subjected to centrifugation (10,000×*g* for 10 min). The resulting supernatant fluid was collected to measure the concentration of unbound proteins. The pellet obtained from centrifugation was resuspended in 1 mL of phosphate buffer solution. A10 μL aliquot of the suspension was used to quantify the total bound and intracellular proteins. The quantification of total proteins in each sample fraction was performed using Qubit™ Protein Assay Kit (Invitrogen, USA) and a Qubit ^{R} 2.0 Fluorometer without protein isolation.

To extract the total DNA concentration from biofilm samples, the QIAamp Viral RNA Kit (Qiagen, USA) was used. The QIAamp Viral RNA Mini Kit can extract small quantities of viral RNA and cellular DNA if both are present in the sample. The biofilm suspension (900 μL) was concentrated by centrifugation at 10,000×*g* for 10 min. Supernatant fluid was decanted. Phosphate buffer solution was added to the pellet to a final volume of 140 μL. The subsequent extraction by the QIAamp Viral RNA Kit was done according to the manufacturers protocol. Quantification of DNA was conducted using Qubit™ 1*X* dsDNA HS (High Sensitivity) Assay Kit (Invitrogen, USA) and Qubit R 2.0 Fluorometer.

3. Results and discussion

3.1. Coating thickness

The AFM analysis of the glass surfaces coated with only polymer and nanoparticles + polymer was performed to measure the mean thickness of coating material. Fig. 3 shows top view images of glass surface coated with only polymer (Fig. 3 a_1), and nanoparticles + polymer (Fig. 3 b_1) as well as the respective corresponding cross-sectional profiles (Fig. 3 a_2 and b_2). As illustrated by the peak in each image, the method of scratching used in analyzing the polymer thickness leaves accumulated residue. Therefore, the reported polymer thickness is the measurement after the residue (test) minus the measurement before the residue (glass). Based on the cross-sectional profiles, the mean thickness of only polymer and nanoparticles + polymer was 151 ± 9 nm and 422 ± 83 nm, respectively.

For this work, the goal was to minimize the polymer thickness applied to the substrate, while ensuring complete coverage of the

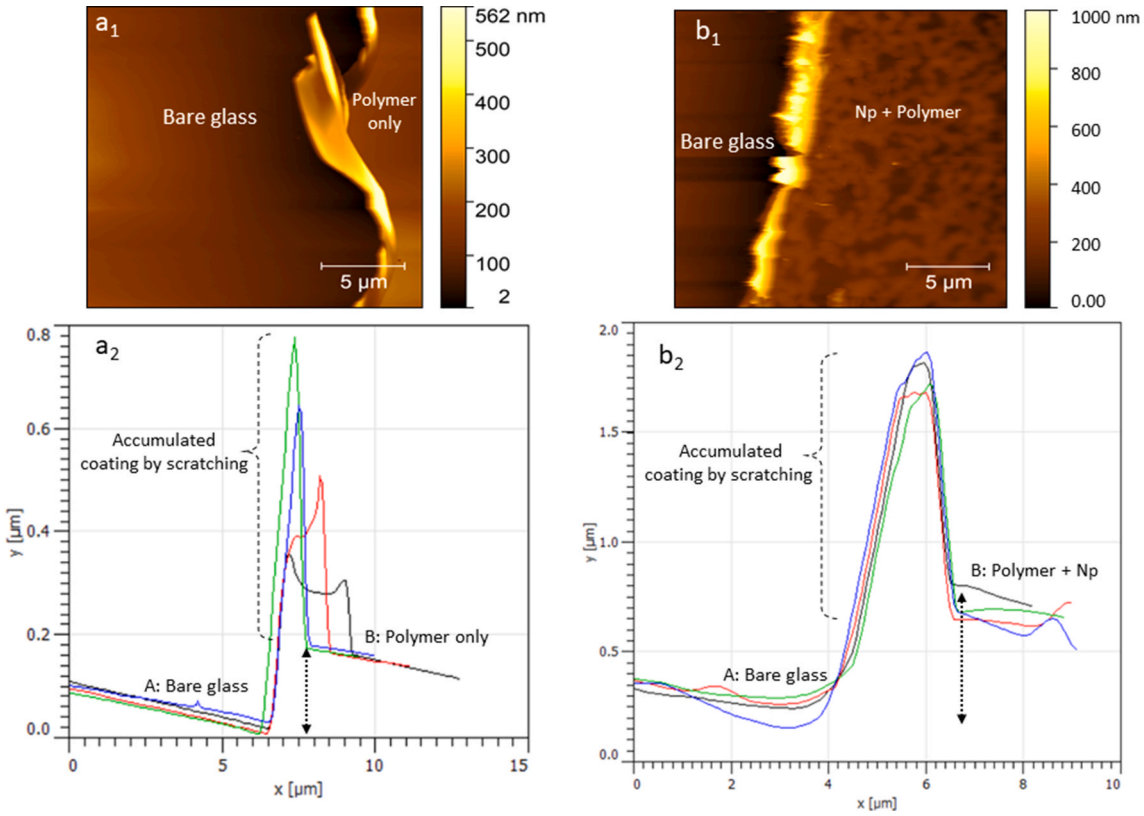

Fig. 3. AFM top view images of glass surface coated with only polymer (a_1) and nanoparticles + polymer (b_1), and corresponding cross-sectional profiles (a_2 and b_2).

substrate and nanoparticles. The polymer thickness should not have a strong effect on the UV performance of the UEGs due to the high transparency of >95% for 1 mm thickness of material. However, the thickness and method of polymer application will affect both the durability and cost of the UEGs. Therefore, an optimization study will be conducted before long-term (>1 month) deployment in future research.

3.2. *Scattering nanoparticles enables glasses to emit UVC light along entire surface*

To obtain effective UVC emission across their surface, UEGs were fabricated using 200 nm silica spheres as scattering particles. Our previous study [20] demonstrated that silica spheres >200 nm coated optical fibers resulted in a UV emission of ~4.4 μW/cm^2. This value was slightly greater than the emission by 100 nm diameter particles (3.4 μW/cm^2), and more than 5-times greater than the emission of 50 nm spheres [20].

Fig. 4 shows the UV irradiance profile through the length of the slides coated with different concentrations of nanoparticles without (Fig. 4 a) with and a secondary polymer coating (Fig. 4 b). In a homogeneous longitudinal waveguide, the intensity of the scattering light follows an exponential decrease (Eq. (1)) [25]:

$$I_r(z) = I_i e^{-\alpha z} \tag{1}$$

where I_R (z) represents the intensity of light remaining in the waveguide at any axial position z; I_i is the amount of light that enters the slide at the $z = 10$ mm; and α is the attenuation coefficient. α is a function of the optical and physical properties of the glass and the surface coating. The attenuation coefficient is a metric for quantifying the decrease in light intensity resulting from the combined effect of scattering and absorption over a given unit length of travel in an attenuating medium {$\alpha = \alpha_s$ (scattering coefficient) + α_a (absorption coefficient)}. SiO_2 has low absorption at UVC range due to its insulation characteristics. The bandgap

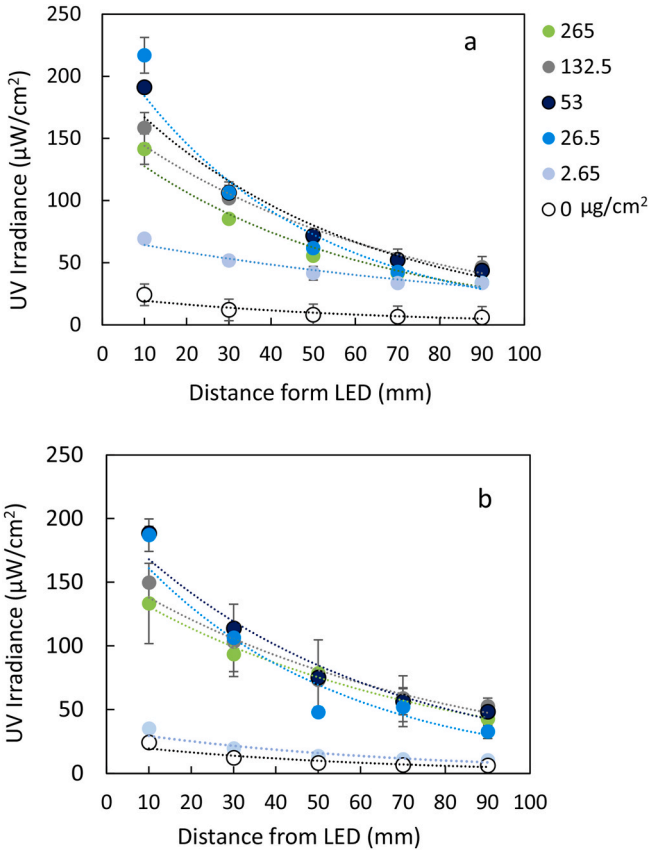

Fig. 4. UV irradiance measurements for slides coated with different concentrations of nanoparticles with (a) and without (b) polymer coating.

energy of SiO_2 falls between 7.52 and 9.6 eV [26]. The photon energy of 4.67 eV in 265 nm wavelength cannot be absorbed and will not be able to excite enough the valence band electrons to jump into the conduction band. Since most of the attenuation is a result of light being scattered from the glass ($\alpha = \alpha_s$), the same equation was used to represent the scattering attenuation of UV light over the length of the glass slide.

The scattering attenuation coefficients for each concentration of nanoparticle coated slide were determined by exponentially fitting the scattering intensity profiles (Fig. 4) and are presented in Table 2. As illustrated, the UV irradiances increases along the slide surface as concentration of nanoparticles increases from 0 to 26.5 μg/cm^2. Greater concentrations led to an insignificant (p-value >0.05, paired *t*-test) change in scattering attenuation coefficient. As previously explained, scattering particles interact with the evanescent wave created at the core surface of the waveguide. Evanescent waves refer to the electromagnetic disturbance that occurs due to total internal reflection at the interface of a transmitting medium [22]. The wave amplitude decreases exponentially with the distance from the interface. Greater concentration of nanoparticles would result in higher wave interaction. These mechanisms have been previously explained in detail for UV Side Emitting Optical Fibers (UV SEOFs) [23,27]. However, increasing the concentration of nanoparticles also results in more light refraction back towards the core of the waveguide instead of being emitted outwards. This can reduce the light that can be used in disinfection.

Fig. 4 b illustrates the UV profile after a polymer layer was added to the slides. There was no statistically significant variation in UV irradiance after polymer coating of UEGs prepared at 26.5–265 μg/cm^2 of nanoparticles. However, a more than 50% decrease in UV irradiance was observed for UEG prepared with a nanoparticle concentration of 2.65 μg/cm^2. Such decrement can result from decreased interaction between nanoparticle and glass slide after the polymer is introduced and was discernible at lower concentration of nanoparticles. Glass slides were coated by electrostatic attachment of positively charged aminated SiO_2 nanoparticles to the negatively charged glass surface. In this process, electrostatic interaction results in the proximity and attachment between nanoparticle and glass surface. The negatively charged polymer can weaken the interaction between glass and nanoparticles and therefore, increase the distance between the two. This phenomenon would result in a decrease in UV emission after polymer application. On the other hand, although CYTOP is an ultra-high UV transparent (over 95%) polymer, it can absorb a small amount of UV irradiation, contributing to the decrease in UV emission.

Fig. 5 depicts the UV irradiance profile and spectral output for the final configuration of UEGs. After waterproofing the case with silicone binder, the UV irradiance decreased by approximately 70% from its original output. Since the scattering attenuation coefficient remained unchanged ($\alpha_s = 0.021$), it can be concluded that the only change was in the light availability, likely due to the addition of silicone as a water barrier. Silicone has a higher index of refraction than the glass slide. Therefore, when light encounters the silicone, it is refracted out of the slide.

3.3. Nanoparticle concentration affects optical transparency of the glass

The transparency of the coated slides was a crucial consideration in this work. Fig. 6 presents transmission spectra of glass slides that were coated with different concentrations of nanoparticles, for both slides coated with and without polymer. Slides coated with 2.65 μg/cm^2 of nanoparticles exhibited a visible light transparency of >95 %, which was comparable with the transparency of the control slide. Visible light transmittance decreased to 74.96 % with increasing the concentration of nanoparticles from 26.5 to 265 μg/cm^2 (Fig. 6 a). Since silica nanoparticles are transparent in the visible spectral region, the decreased light transmission by increasing the silica nanoparticles concentration is attributed to the strong light scattering, including resonant and random scattering, on the surfaces of the silica nanoparticles [28]. As illustrated, the addition of a transparent polymer coating did not increase the light transmittance in the visible region of the slides with concentration of 2.65 and 265 μg/cm^2 of nanoparticles. However, polymer coating increased transmittance of the slides by 13, 3.3, and 16.6 % for nanoparticle concentrations of 26.5, 53, and 132.5 μg/cm^2 respectively (Fig. 6 b). This increase in transparency upon polymer addition can be

Table 2
Values of scattering attenuation coefficients for slides coated with different concentrations of nanoparticles, with and without polymer coating.

Polymer coating	Dilution value of nanoparticles					
	0 to 1	1 to 0	1 to 2	1 to 5	1 to 10	1 to 100
Yes	0.017	0.014	0.013	0.017	0.021	0.015
No	0.017	0.018	0.016	0.018	0.023	0.009

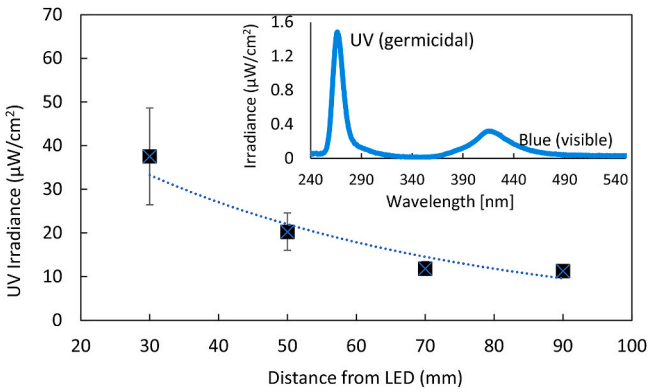

Fig. 5. The final UV emission profile and the UV spectrum (inset) for UEG used in submersion.

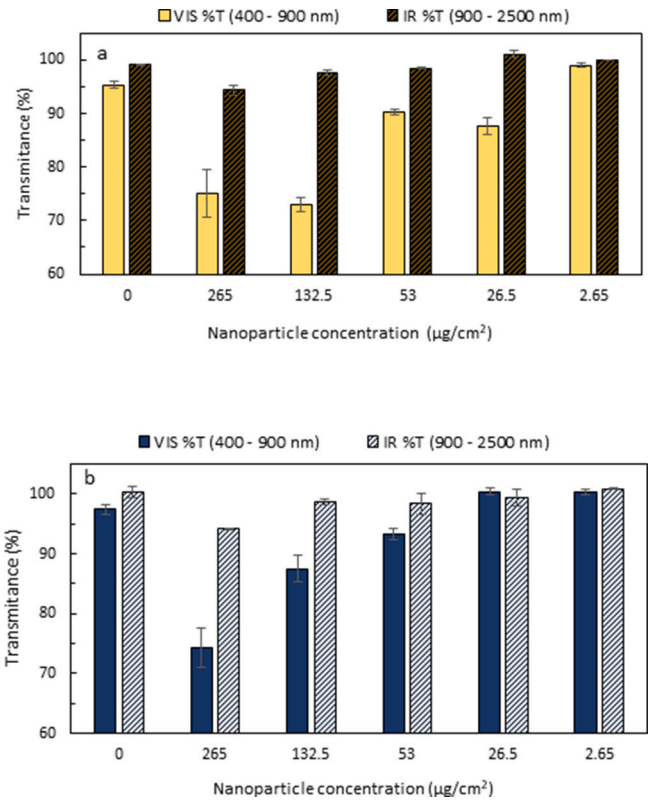

Fig. 6. Transparency of slides coated with different concentrations of nanoparticles without (a), and with (b) polymer coating.

due to the decrease in the scattering of visible light. Rayleigh theory describes the reduction of light intensity due to scattering in nanoparticles-polymer composites. This theory was expressed by Novak [29] through equation (2):

$$\frac{I}{I_i} = e^{-\left[\frac{3\ V_p\ x\ r^3}{4\lambda^4}\left(\frac{n_p}{n_m}-1\right)\right]} \quad (2)$$

where, I represents the intensity of the transmitted light by the nanoparticle-polymer composite, while V_p and r are the volume fraction and radius of the particles, respectively. In this equation, x is the optical path length, λ is the wavelength, while n_p and n_m represent the refractive index of nanoparticles and polymer matrix, respectively.

According to equation (2), if $n_p = n_m$, the scattering is zero, and the transmission is equal to 1 (T = 100%). The intensity of scattered light by silica nanoparticles ($n_p = 1.43$) at visible region can be decreased by a polymer matrix ($n_m = 1.34$ for CYTOP polymer), resulting in greater transparency.

As indicated by Equation (2), increasing the thickness of the coating results in an extended optical path length, that can therefore lead to a reduction in transparency. We assume that, in general, thicker coatings would significantly decrease the UV transparency. However, because the polymer has >95% transparency for a path length of 1 mm, changes in UV emission due to polymer thickness were negligible. Every slide tested transmitted more light in the NIR region as compared to the visible region. In the visible region, the light transmittance of the slides used for submersion (concentration of nanoparticles: 26.5 μg/cm^2) was 88 ± 1.6% without polymer coating and 100.4 ± 0.6% with the polymer coating. Light transmission in the NIR region was 101 ± 0.6% without polymer coating and 99.4 ± 1.3% with polymer coating. Data exceeding 100 % are attributed to experimental errors in the instrumentation. These results suggest that the UEG used in this study would excel transparency performance criteria for both visible and near-infrared applications.

Resolving power is another important feature of transparent surfaces. This is the ability of an instrument or the human eye to distinctly differentiate between two objects positioned closer than the minimum angular separation discernible to the observer's eye. All tested slides, coated with different concentrations of nanoparticle and with or without polymer, exhibited 100 % resolving power (versus blank) and excellent optical clarity (data are not shown).

3.4. Biofilm prevention by UEG

3.4.1. UEG decreases biofilm coverage

Fig. 7 an illustrates the photographs of the control slides and UEGs that were submerged and exposed to continuous UVC radiation for 20 days. Visual assessment results (Fig. 7 b) indicated a reduction of over 92% in biofilm coverage on UEGs compared to the control slides. The slides modified with scattering particles delivered more than 7.7 times the UVC dose and achieved 13.7-fold less biofilm coverage compared to the control slides. Most of the observed growth was unidentified microorganism biofouling, green algae, and amphipod tubes.

The culturable cells attached to the surface of each slide were quantified as CFU and are presented in Fig. 8a. On average, the control slides exhibited CFU counts of about 1000 ± 190, 700 ± 280, and 600 ± 310 CFU/cm^2 for p_1, p_2, and p_3 sections, respectively. In contrast, the UEGs showed significantly lower CFU counts, with only 10 ± 2.7 CFU/cm^2 for p_1, 12 ± 6.6 CFU/cm^2 for p_2, and 16 ± 5.5 CFU/cm^2 for p_3. Although a descending trend in CFU was expected with increasing the distance from the UVC source, no statistically significant (p-value >0.05, paired *t*-test) difference in biofilm abundance was observed among the across three sections of the slides, suggesting proximity to the light source did not impact biofilm mitigation. The average UV dose for section p_3 totaled approximately 19.56 J/cm^2 for 20 days of submersion, with an irradiance of 11.32 μW/cm^2 (Fig. 5). This dose and irradiance were highly effective in preventing biofilm attachment and growth on the surface resulting in 1.79 log reduction of biofilm in comparison to the control.

The required UV dose for effective inactivation of planktonic bacteria can vary from the dose necessary for surface disinfection. For example, a dose of 25 J/cm^2 was found to be effective in biofouling control and 1 log inactivation of *Navicula incerta* cells on a UV-lucent silicone integrated with UVC LEDs [30]. Torkzadeh et al. [12] observed that a UV dose of 8.7 J/cm^2 at 254 nm achieves 1.3 log inactivation corresponding to 95 % decrease in *E. coli* surface biovolume, while a 0.02 J/cm^2 dose was sufficient for approximately 5 log inactivation of planktonic *E. coli*. Bacteria in biofilms are physiologically and morphologically different from their planktonic growing counterparts. Once bacteria attach to a surface and begin producing EPS, they become highly resistant to disinfection. Additionally, marine bacteria, due to their aggressive adaptation to harsh oceanic conditions, can require more intensive irradiation for effective biofilm control. On the other hand, the accumulation of sediment and organic materials on the surfaces can act as a shield for biofilms exposed to UV irradiation, affecting

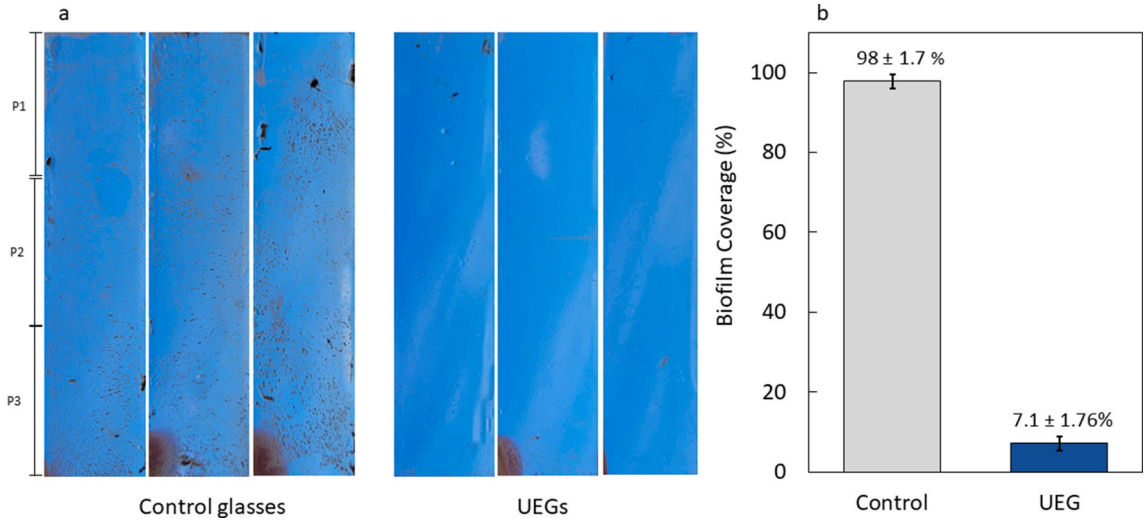

Fig. 7. Photographs (a) and relative abundance (b) of biofilm coverage on the control and UEG after immersion for 20 days. The data presented are the average values of 4 control slides and 8 UEGs submerged in two cases.

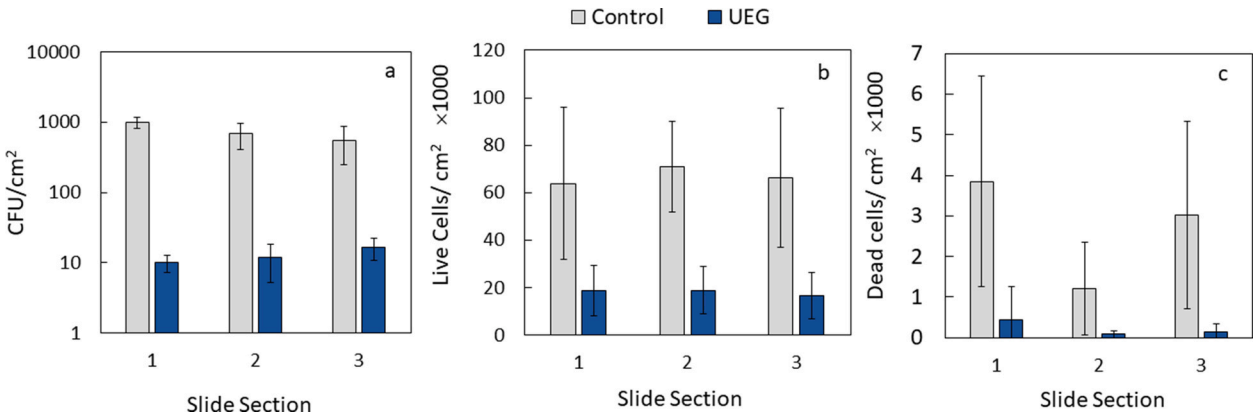

Fig. 8. Number of CFU (a) live (b), and dead cells (c) in UEG compared to control slides after immersion for 20 days. The data presented are the average values of 4 control slides and 8 UEGs submerged in two cases.

UV transmission [16]. Therefore, a higher UV intensity would be required for the effective removal of the biofilms formed in the marine environment.

3.4.2. Lower viable cell count in UEG

The LIVE/DEAD BacLight Bacterial Viability Kit was employed to assess the viability and distribution of live and dead cells within the biofilm samples. In this method, membrane integrity is considered the criterion to differentiate viable bacterial cells from dead ones. Viable cells are assumed to have intact and impermeable cell membranes that prevent the penetration of certain staining compounds, whereas dead cells are recognized by their disrupted or broken membranes [31].

Microscopy analysis of the samples revealed the presence of microcolonies and individual cells within the biofilm samples. A small number of dead cells were observed, along with amorphous red propidium iodide-stained material, which can represent DNA-containing debris from lysed cells. In the biofilm grown on the UEGs, the number of cells exhibiting both live and dead fluorescence was limited, and these cells were sporadically distributed. Live and dead cells were counted separately for the control slides and UEGs and the results are illustrated in Fig. 8 b and c respectively. Comparable to the results obtained from the pour-plate method, no significant difference (p-value >0.05, paired-t-test) in the number of live/dead cells was observed among different sections of the slides. On average, the number of live bacterial cells in the biofilm grown on the UEGs was found to be 73 ± 2.1% lower than that on control slides. The number and proportion of dead cells in biofilm grown on UEG was also lower than that of control slides (Fig. 8 c).

In addition, live:dead ratio was 82:1 and 25:1 for biofilm grown on UEG and control slides, respectively. This can result from the mode of action of the LIVE/DEAD Baclight stains being incongruous with the UV inactivation mechanism. The LIVE/DEAD BacLight method allows for the detection of cell states beyond just live and dead cell. This includes identification of live injured cells that are unable to grow on agar plates [32–34]. Germicidal UVC prevents the buildup of bacterial biofilms via breaking the chemical bonds between DNA and RNA polymers within microorganisms, disrupting the genetic code, and preventing DNA from replicating [35,36]. However, since UVC does not directly affect membrane integrity [12], many metabolically inactivated cells did not stain red, as their membranes were still intact. Consequently, the number of live cells estimated using this method is noticeably greater than the counts obtained from the pour-plate method. It can be concluded that the pour plate method can be a more accurate technique for quantifying the viable bacteria in UV-irradiated biofilm.

3.4.3. Protein and DNA analysis

DNA and proteins are two of the main molecules identified in natural marine biofilms that are essential for biofilm growth and survival. The

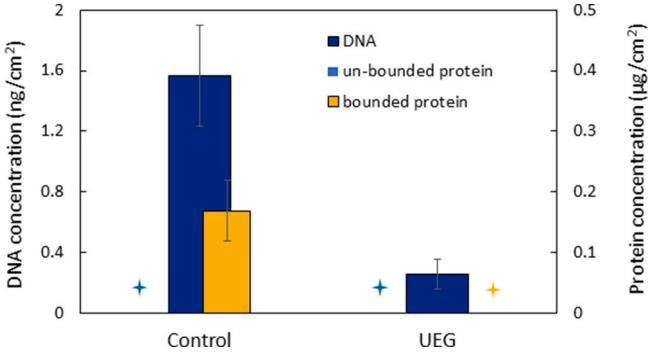

Fig. 9. Concentration of total DNA, unbound, and bound protein in biofilm samples after immersion for 20 days.

total DNA unbound, and bound protein concentrations were determined on each UEG and control slide and are illustrated in Fig. 9. The mean value of total DNA concentration for control and UEG slides were 1.6 ± 0.33 ng/cm^2, and 0.2 ± 0.1 ng/cm^2, respectively. These results align with the number of CFU observed in both control and UEG slides. UVC radiation particularly targets nucleic acid molecules, and it interacts with bacterial DNA to inhibit growth, reproduction, and the formation of biofilms [37]. It is worth noting that an increased cell density in the biofilm corresponds to a greater concentration of DNA.

The concentration of bound proteins in the control slides was 0.17 ± 0.05 µg/cm^2. However, bound proteins concentration was below detection in the UEGs. Additionally, concentration of unbound proteins was below detection on all slides. It is likely that the reconstituted concentration of proteins in these samples fell below the detection limit of the method employed. It should be noted that UVC has been reported to irreversibly damage proteins and prevent enzymatic DNA repair processes [38]. Proteins are a crucial component of extracellular polymeric substances (EPS) and, together with polysaccharides, play a vital role in the structural properties of biofilms due to their gel like nature [39].

3.5. Further development of UEGs

This proof-of-concept study demonstrated the use of UEGs for prevention of biofilm growth on transparent surfaces. However, there are still significant limitations for a broad application and adaptation of UEG in biofilm prevention. The main limitation of the current work is that only a 20 day submersion period was assessed using relatively small substrates. This means that issues with longevity and limitations in preventing biofilm growth over larger areas could not be assessed. The

two main areas of development foreseen to be needed include (1) long-term stability and performance of UEGs, and (2) the light distribution profile across larger surface areas. In relation to (1) engineering the design related to polymer thickness and application methods will enable the polymer coating to be durable during long-term submersion. Specifically, these improvements will reduce potential for delamination and damage from general use or cleaning procedures. Related to (2), a better modeling of light distribution across the waveguide (e.g. using ray-tracing approaches) will inform the design of each specific UEG to enable a minimum irradiation for biofilm prevention. Both nanoparticle concentration and LED coupling configurations can be modified to achieve these design requirements. Additionally, more work has to be done to understand the advantages and disadvantages of UEGs in comparison to both conventional external UVC radiation techniques and other biofilm prevention approaches (e.g. antifouling coatings). External UVC irradiation inhibits biofilm formation by inactivating planktonic microorganisms prior to attachment. UEGs inhibit biofilm formation directly at the surface of interest during all stages of attachment and growth. Contrary to external exposure, the surface itself serves as a UVC source. Furthermore, it is worthwhile to compare the effectiveness of UEGs with other antifouling coating techniques, such as surface modifications. Quantifying an energy budget that accounts for both capital and operational costs associated with these technologies enables comparison between these strategies.

4. Conclusion

This study showcases the promising potential of employing UEGs for inhibition of biofilm growth on transparent surfaces. We determined that the concentration of nanoparticles plays a pivotal role in scattering UVC light. A concentration of 26.5 μg/cm^2 was selected to maximize UV irradiance intensity, while prioritizing substrate visible light transparency. The novel scattering nanoparticle coated glass surfaces exhibited remarkable inhibitory effects on biofilm growth reducing visible biofilm coverage by 92 % and culturable cell count by over 98% based on number of CFU, during 20 days of marine submersion. Detailed microscopic analysis also revealed lower viable cell counts within the biofilm grown on the modified surfaces. These results not only underscore the potential for UEGs to enhance surface hygiene and mitigate microbial contamination but also open new avenues for their utilization in diverse disinfection applications. The described UEG can be used for disinfection of transparent surfaces such as windows of ships, flotation spheres and moored buoys, camera lenses and sensors for oceanographical, agricultural, water treatment, and process design applications.

CRediT authorship contribution statement

Leila Alidokht: Writing – original draft, Methodology, Investigation, Formal analysis, Data curation. **Katrina Fitzpatrick:** Writing – review & editing, Validation, Methodology. **Caitlyn Butler:** Writing – review & editing, Supervision, Methodology, Investigation, Funding acquisition. **Kelli Z. Hunsucker:** Writing – review & editing, Methodology. **Cierra Braga:** Writing – review & editing, Methodology. **William A. Maza:** Writing – review & editing, Methodology. **Kenan P. Fears:** Writing – review & editing, Methodology. **Marieh Arekhi:** Writing – review & editing. **Mariana Lanzarini-Lopes:** Writing – review & editing, Writing – original draft, Supervision, Resources, Project administration, Methodology, Investigation, Funding acquisition, Conceptualization.

Declaration of competing interest

The authors declare the following financial interests/personal relationships which may be considered as potential competing interests: Mariana Lanzarini-Lopes reports a relationship with Optical Waters that includes: board membership, equity or stocks, and funding grants. Katrina Fitzpatrick reports a relationship with Optical Waters that includes: board membership, equity or stocks, and funding grants. If there are other authors, they declare that they have no known competing financial interests or personal relationships that could have appeared to influence the work reported in this paper.

Data availability

Data will be made available on request.

Acknowledgments

We express our gratitude to Daniel A. Steinhurst for writing scripts and providing valuable assistance in the development of experimental procedures for optical transparency measurements. Our appreciation goes to Dave Follette for his support in case design and the 3D printing service and to Evan Patamia for his support on AFM imaging and analysis. We extend our thanks to Violumas Co, San Diego, CA, for providing the UVC LED strips and technical support that greatly contributed to this study. Furthermore, we acknowledge the funding support for this project provided by the Office of Naval Research (ONR) to UMass Amherst (Grants #N00014-22-1-2540 and N00014-23-1-2448) and the Florida Institute of Technology (Grant #s N00014-20-1-2214 and N00014-20-1-2243.

References

[1] Schultz MP, Bendick JA, Holm ER, Hertel WM. Economic impact of biofouling on a naval surface ship. Biofouling 2011;27(1):87–98. https://doi.org/10.1080/08927014.2010.542809.
[2] Li C, Atlar M, Haroutunian M, Norman R, Anderson C. An investigation into the effects of marine biofilm on the roughness and drag characteristics of surfaces coated with different sized cuprous oxide (Cu2O) particles. Biofouling 2019;35(1):15–33. https://doi.org/10.1080/08927014.2018.1559305.
[3] Tamburri MN, Davidson IC, First MR, Scianni C, Newcomer K, Inglis GJ, Georgiades ET, Barnes JM, Ruiz GM. In-water cleaning and capture to remove ship biofouling: an initial evaluation of efficacy and environmental safety. Front Mar Sci 2020;7. https://doi.org/10.3389/fmars.2020.00437.
[4] Almeida E, Diamantino TC, de Sousa O. Marine paints: the particular case of antifouling paints. Prog Org Coating 2007;59(1):2–20. https://doi.org/10.1016/j.porgcoat.2007.01.017.
[5] Salta M, Goodes LR, Maas BJ, Dennington SP, Secker TJ, Leighton TG. Bubbles versus biofilms: a novel method for the removal of marine biofilms attached on antifouling coatings using an ultrasonically activated water stream. Surf Topogr 2016;4(3):034009. https://doi.org/10.1088/2051-672X/4/3/034009.
[6] Pistone A, Scolaro C, Visco A. Mechanical properties of protective coatings against marine fouling: a review. Polymers 2021;13(2):173. https://doi.org/10.3390/polym13020173.
[7] Torkzadeh H, Cates EL. Biofilm growth under continuous UVC irradiation: quantitative effects of growth conditions and growth time on intensity response parameters. Water Res 2021;206:117747. https://doi.org/10.1016/j.watres.2021.117747.
[8] Dai TianHong Dai TianHongand Vrahas, M. S. and M. C. K. and H.M. R. Ultraviolet C irradiation: an alternative antimicrobial approach to localized infections? 10 (2), 185–195..
[9] Lanzarini-Lopes M, Cruz B, Garcia-Segura S, Alum A, Abbaszadegan M, Westerhoff P. Nanoparticle and transparent polymer coatings enable UV-C side-emission optical fibers for inactivation of Escherichia coli in water. Environ Sci Technol 2019;53(18):10880–7. https://doi.org/10.1021/acs.est.9b01958.
[10] Senevirathne SWMAI, Toh YC, Yarlagadda PKDV. Fluid flow induces differential detachment of live and dead bacterial cells from nanostructured surfaces. ACS Omega 2022;7(27):23201–12. https://doi.org/10.1021/acsomega.2c01208.
[11] Gora SL, Rauch KD, Ontiveros CC, Stoddart AK, Gagnon GA. Inactivation of biofilm-bound Pseudomonas aeruginosa bacteria using UVC light emitting diodes (UVC LEDs). Water Res 2019;151:193–202. https://doi.org/10.1016/j.watres.2018.12.021.
[12] Torkzadeh H, Zodrow KR, Bridges WC, Cates EL. Quantification and modeling of the response of surface biofilm growth to continuous low intensity UVC irradiation. Water Res 2021;193. https://doi.org/10.1016/j.watres.2021.116895.
[13] Richard KN, Hunsucker KZ, Gardner H, Hickman K, Swain G. The application of UVC used in synergy with surface material to prevent marine biofouling. J Mar Sci Eng 2021;9(6). https://doi.org/10.3390/jmse9060662.
[14] Ma B, Seyedi S, Wells E, McCarthy D, Crosbie N, Linden KG. Inactivation of biofilm-bound bacterial cells using irradiation across UVC wavelengths. Water Res 2022;217:118379. https://doi.org/10.1016/j.watres.2022.118379.
[15] Abhishek N, Mark S, H MP. Impacts of UV-C irradiation on marine biofilm community succession. Appl Environ Microbiol 2022;88(4):e02298-21. https://doi.org/10.1128/aem.02298-21.

[16] Braga CR, Richard KN, Gardner H, Swain G, Hunsucker KZ. Investigating the impacts of UVC radiation on natural and cultured biofilms: an assessment of cell viability. Microorganisms 2023;11(5). https://doi.org/10.3390/microorganisms11051348.
[17] Braga C, Hunsucker K, Gardner H, Swain G. A novel design to investigate the impacts of UV exposure on marine biofouling. Appl Ocean Res 2020;101:102226. https://doi.org/10.1016/j.apor.2020.102226.
[18] Cagnola GN, Cabrera JN, Negri RM, D'Accorso NB, Lizarraga L, Pettinari MJ. Biofilm Formation of two different marine bacteria on modified PDMS surfaces is affected by surface roughness and topography. Curr Microbiol 2023;80(8):256. https://doi.org/10.1007/s00284-023-03370-5.
[19] Ryan E, Turkmen S, Benson S. An investigation into the application and practical use of (UV) ultraviolet light technology for marine antifouling. Ocean Eng 2020;216:107690. https://doi.org/10.1016/j.oceaneng.2020.107690.
[20] Lanzarini-Lopes M, Garcia-Segura S, Hristovski K, Messerly M, Simon AJ, Westerhoff P. Particle-modified polymeric cladding on glass optical fibers enhances radial light scattering. J Opt Soc Am B 2019;36(6):1623–8. https://doi.org/10.1364/JOSAB.36.001623.
[21] Chew H, Wang D-S, Kerker M. Elastic scattering of evanescent electromagnetic waves. Appl Opt 1979;18(15):2679–87. https://doi.org/10.1364/AO.18.002679.
[22] Prieve DC, Walz JY. Scattering of an evanescent surface wave by a microscopic dielectric sphere. Appl Opt 1993;32(9):1629–41. https://doi.org/10.1364/AO.32.001629.
[23] Lanzarini-Lopes M, Zhao Z, Perreault F, Garcia-Segura S, Westerhoff P. Germicidal glowsticks: side-emitting optical fibers inhibit Pseudomonas aeruginosa and Escherichia coli on surfaces. Water Res 2020;184. https://doi.org/10.1016/j.watres.2020.116191.
[24] ASTM. D6990 standard practice for evaluating biofouling resistance and physical performance of marine coating systems. West Conshohocken: ASTM International; 2020. p. 13. https://doi.org/10.1520/D6990-20. https://www.astm.org/d6990-20.html.
[25] Elvis Cao X, Hong T, Hong S, Erickson D. Engineering waveguide surface by gradient etching for uniform light scattering in photocatalytic applications. Chem Eng J Adv 2021;8. https://doi.org/10.1016/j.ceja.2021.100192.
[26] Altman IS, Lee D, Chung JD, Song J, Choi M. Light absorption of silica nanoparticles. Phys Rev B 2001;63(16):161402. https://doi.org/10.1103/PhysRevB.63.161402.
[27] Zhao Z, Lanzarini-Lopes M, Westerhoff E, Long X, Rho H, Bi Y, Ling L, Westerhoff P. Evanescent wave interactions with nanoparticles on optical fiber modulate side emission of germicidal ultraviolet light. Environ Sci Nano 2021;8(9):2441–52. https://doi.org/10.1039/D1EN00199J.
[28] Dai X, Rasamani KD, Hall G, Makrypodi R, Sun Y. Geometric symmetry of dielectric antenna influencing light absorption in quantum-sized metal nanocrystals: a comparative study. Front Chem 2018;6.
[29] Novak BM. Hybrid nanocomposite materials—between inorganic glasses and organic polymers. Adv Mater 1993;5(6):422–33. https://doi.org/10.1002/adma.19930050603.
[30] Whitworth P, Aldred N, Reynolds KJ, Plummer J, Duke PW, Clare AS. Importance of duration, duty-cycling and thresholds for the implementation of ultraviolet C in marine biofouling control. Front Mar Sci 2022;8. https://doi.org/10.3389/fmars.2021.809011.
[31] Grégori G, Denis M, Sgorbati S, Citterio S. Resolution of viable and membrane-compromised free bacteria in aquatic environments by flow cytometry. Curr Protoc Cytom 2018;85(1):e42. https://doi.org/10.1002/cpcy.42.
[32] Davis C. Enumeration of probiotic strains: review of culture-dependent and alternative techniques to quantify viable bacteria. J Microbiol Methods 2014;103:9–17. https://doi.org/10.1016/j.mimet.2014.04.012.
[33] Stiefel P, Schmidt-Emrich S, Maniura-Weber K, Ren Q. Critical aspects of using bacterial cell viability assays with the fluorophores SYTO9 and propidium iodide. BMC Microbiol 2015;15(1):36. https://doi.org/10.1186/s12866-015-0376-x.
[34] Léonard L, Bouarab Chibane L, Ouled Bouhedda B, Degraeve P, Oulahal N. Recent advances on multi-parameter flow cytometry to characterize antimicrobial treatments. Front Microbiol 2016;7. https://doi.org/10.3389/fmicb.2016.01225.
[35] Cates EL, Cho M, Kim J-H. Converting visible light into UVC: microbial inactivation by Pr3+-activated upconversion materials. Environ Sci Technol 2011;45(8):3680–6. https://doi.org/10.1021/es200196c.
[36] Craik SA, Finch GR, Bolton JR, Belosevic M. Inactivation of giardia muris cysts using medium-pressure ultraviolet radiation in filtered drinking water. Water Res 2000;34(18):4325–32. https://doi.org/10.1016/S0043-1354(00)00207-4.
[37] Chevremont A-C, Farnet A-M, Sergent M, Coulomb B, Boudenne J-L. Multivariate optimization of fecal bioindicator inactivation by coupling UV-A and UV-C LEDs. Desalination 2012;285:219–25. https://doi.org/10.1016/j.desal.2011.10.006.
[38] Nyangaresi PO, Qin Y, Chen G, Zhang B, Lu Y, Shen L. Effects of single and combined UV-LEDs on inactivation and subsequent reactivation of E. Coli in water disinfection. Water Res 2018;147:331–41. https://doi.org/10.1016/j.watres.2018.10.014.
[39] Yu H-Q. Molecular insights into extracellular polymeric substances in activated sludge. Environ Sci Technol 2020;54(13):7742–50. https://doi.org/10.1021/acs.est.0c00850.